Advances in Science and Technology Research Journal

*Advances in Science and Technology Research Journal*, 2026, 20(2), 78–93
https://doi.org/10.12913/22998624/211078
ISSN 2299-8624, License CC-BY 4.0

Received: 2025.09.23
Accepted: 2025.11.19
Published: 2025.12.23

# Study on the resistance to friction in a lead screw-nut contact zone in a car scissor lift

Marek Woźniak[1], Jakub Morawski[2], Sergiusz Zakrzewski[1], Arkadiusz Kądziela[1], Tomasz Szydłowski[1], Krzysztof Siczek[1*], Szymon Szufa[3]

[1] Department of Vehicles and Fundamentals of Machine Design, Lodz University of Technology, ul. Stefanowskiego 1/15, 90-537 Lodz, Poland
[2] Mechanical Faculty, Lodz University of Technology, ul. Stefanowskiego 1/15, 90-537 Lodz, Poland
[3] Faculty of Process and Environmental Engineering, Lodz University of Technology, ul. Wólczańska 213, 93-005 Lodz, Poland
* Corresponding author's e-mail: ks670907@p.lodz.pl

## ABSTRACT

This study aimed to investigate the resistance to friction in the lead screw-nut contact zone of a car scissor lift during operation. In both cases of a lack of lubricant and a lubricated contact zone, the stick-slip phenomenon occurred therein. The analytical model of the lead screw-nut assembly driven by an electric motor was elaborated. During the operation of such an assembly, lubricated stick-slip oscillations occurred with smaller magnitudes compared to the case of dry friction in the contact zone. During lifting the vehicle, the friction torque values in the lead screw-nut contact zone lowered due to lowered contact pressure caused by the lowered value of the force loading the contact zone due to changing values of the angle between the lead screw and the lift arm. Contrary, during lowering the vehicles, the friction torque values in the lead screw-nut contact zone slightly increased. In the case of polytetrafluoroethylene (PTFE)-based lubricant, the values of the friction torque less than half of those for dry/boundary friction conditions in the analyzed contact zone. The use of lithium grease further halved the friction torque values compared to the case of the PTFE-based lubricant.

**Keywords:** car scissor lift, friction coefficient, lubricant.

## INTRODUCTION

Lifting devices are widely used in the automotive industry to raise, lower, and move vehicles. Scissor lifts are often utilized for this purpose [1, 2]. Specifically, the current service, brakes and suspension use a mobile scissor lift raising tires to a height of up to 1 meter. Additionally, the scissor lift mounted on the duct is suitable for all repair operations except for replacing the fuel filter, and for sheet metal work [3]. According to [4], the scissor lift is for work under the vehicle and for wheel alignment. Scissor lifts often utilize hydraulic drives [5]. According to [6], scissor lifts can be either drive-on or four-arm style lifts. Hongyu and Ziyi [7] reported that the scissor lift platform consists of the main platform for lifting, a lift mechanism with the scissors posts and the hydraulic cylinders, along with a mobile self-propelled base providing traction. The platform is equipped with two pairs of scissors.

An automatic scissor jack for cars is designed to elevate vehicles with minimal manual input. It generally employs a 12V DC motor to turn a power screw, extending the scissor mechanism and lifting the vehicle. These jacks frequently include features such as automatic halting at a set height and can be operated via a remote or smartphone [8–10]. Automatic scissor jacks may comprise the sub-devices that enable automatic stopping at a pre-set height, preventing over-extension and potential damage [11]. Babu et al. [12] created and constructed a power scissor jack capable of raising and holding a load of 4.5 kN for standard applications in

four-wheel vehicles. The sizes of different parts were standardized for convenient assembly and replacement, if necessary. The self-weight of the power jack was reduced for easier handling.

Ajayi and Adeyinka [13] obtained an automatic scissor screw car jack by adding a sleeve coupling between the manual screw jack and a 12V DC electric motor, which receives power through a direct current flow from the car battery. Nevertheless, the function of most car jacks is manual and necessitates extended periods of bending or squatting during use, posing challenges for many women, the disabled, the elderly, etc. Primarily, it lacks ergonomic suitability for the human body due to the crouching and squatting postures during operation, potentially leading to health issues. The heavier the vehicle, the more time is needed to raise it off the ground to the specified height with an automatic scissor. Additionally, Pratheep et al. [14] proposed a scissor jack with a lead screw driven manually or with the aid of an electric motor powered from the vehicle battery.

The scissor lift analyzed in the present study can be adapted for manual lifting or gear motor operation owing to interchangeable attachments. However, the current study concerns the latter version. Manual scissor lifts commonly operate under dry friction conditions in contact with the lead screw and nut, while their bearings have close casing comprising various greases, mainly lithium ones. When lifts are driven by motors combined with gears, the latter are lubricated with various oils or greases. Gear teeth operate under the conditions of boundary friction, bearings in the devices operating under start-stop conditions experience mixed friction, as well as the consumption of oil and grease contributes to a more frequent occurrence of boundary friction and even technically dry friction, increasing the resistance to movement. An interesting method to evaluate the boundary layer action deterioration process, in the form of the acoustic emission measurements, was proposed by [15].

Research on screw jacks examines their design [13, 14, 16, 17], functionality, and uses, frequently highlighting efficiency [18, 19], load capacity [16, 17], and user-friendliness [20–22]. These investigations encompass theoretical assessments and simulations [22–27], alongside the creation of prototypes and experimental research [15]. The studies explore, among other topics vehicle elevation [13, 17], farming equipment [25], and factory environments [20]. Foulve [16] designed a special screw jack tailored for lifting lightweight objects up to a 2-ton capacity, particularly useful for small-scale workshops, where precision and controlled lifting of lighter loads are crucial.

Abdulafeez et al. [19] developed a screw jack experimental demonstration allowing understanding of the efficiency of a lifting device and the relationship of effort needed to lift the load. For loads ranging from 50 N to 250 N, the effort increased with load and the efficiency of the screw jack was around 50%. The efficiency and velocity ratio were not constant due to the occurrence of friction in the system. Ezurike and Okwu [20] presented an updated screw jack design that incorporates a crank and bevel gear system to decrease ergonomic stress by lessening the requirement for extended squatting or bending while in use. This redesign reduces operator's back discomfort and enhances operational safety while preserving lifting effectiveness, thus directly addressing the ergonomic shortcomings of traditional screw jacks.

Akinwonmi and Mohammed [21] modified an existing motor screw jack by incorporating an electric motor powering the screw via a gear when electrical power was supplied from the automobile 12V battery. The modification made the operation easier, safer, and more reliable, reducing health risks, especially the backache problems associated with work in a bent or squatting position for an extended period. Shejwal et al. [22] effectively reduced the weight of the screw jack body by thoughtfully adding holes while maintaining load-carrying capacity, thus improving portability and ease of use. Using finite element analysis (FEA), they found that the design preserved structural strength while enhancing user comfort, aiding handling, particularly for women and teenagers.

Patil and Kachave [26] developed the motorized scissor jack of reduced mass and analyzed the stress distribution therein using FEA. Muhammed et al. [23] developed a design procedure for a simple screw jack. Ayai et al. [28] developed a straightforward methodology for the design of the motorized scissor jack. Pervan et al. [27] developed a parametric CAD model of a car jack for the numerical structural analysis of the latter.

Using FEA, Khatwate et al. [24] analyzed a screw jack in terms of total deformation, equivalent stress and factor of safety (FOS) for the power screw to find the most suitable material. The studied materials for the screw included 20Mn2, 35Mn2Mo28, 35Mn2Mo48, C50 and C60. The

materials used for components other than the power screw were grey cast iron for the cup and frame, phosphor bronze for the nut, and stainless steel for the handle. The 35Mn2Mo28 material was the best for the screw.

Using the SimScape multi-body environment, de Simone et al. [25] modeled the kinematics of the non-back-drivable screw jack mechanism for the hitch-lifting arms. Inverse dynamic analyses allowed identification of the characteristics required of the electric motors. The direct dynamic analysis allowed testing the reversible and irreversible behavior of the lifter for an optimal component design.

Tambari et al. [29] experimentally studied the effectiveness of a laboratory screw jack to determine the force ratio (mechanical advantage), velocity ratio and mechanical efficiency of a device under loads varying from 100 N to 450 N. The efficiency of a screw jack was below 50% as the mechanical advantage and velocity ratio were both less than 0.5. The variable efficiency was due to the various loading conditions the machine faces, which involve significant frictional forces between the screw and the threaded base it operates within.

Currently, many lead screws mate with polymer nuts with integral lubricants; however, an alternative is PTFE-based coating of the lead screws, allowing for values of the coefficient of friction in the range of 0.06 to 0.12. When the lead screw mates with the bronze nut (higher loading), the proper screw coating can be the modified $WS_2$ coating or chrome plating. The latter is especially useful for corrosion resistance in marine applications [30].

Sharifov and Bashirov [31] investigated the behavior of the composition and structure of the diffusion of Cr coatings in sliding. They noticed that the strain in friction formed the secondary structure of Cr coatings, and because of the deformation effect, wear intensified due to the separation of the coating.

The goal of the present study was to investigate the resistance to friction in the lead screw-nut contact zone in a chosen car scissor lift operating under dry/boundary conditions and under lubrication by grease of a chosen type. The novelty of the present study is the consideration of the resistance to movement between the screw and the nut both in the lifting and lowering phases, as well as the variation of the force loading the screw during the lifting and lowering process, whereas in the analyzed models described in the literature [22, 23, 32] this force had a relatively constant value, and the consideration of the resistance to movement in the joints between the holes of the moving parts of the scissor lift and the mating surfaces of the pins connecting these parts.

## SCREW JACK MECHANISM

The friction moment in the screw mechanism depends on its friction coefficient (COF), the load of the screw, its pitch and the nominal radius determining the slope of the thread [33] Bronzini [34] pointed out that a trapezoidal screw jack is predestined to move a heavy load with a high degree of accuracy and safety. The choice of a trapezoidal screw jack is affected by load capacity, input speed, duty cycle, and other factors like temperature as well as vibrations affecting the screw jack operations [35]. When lifting a load in a compression configuration, the spindle may be susceptible to buckling or deformation under the weight of the load. In traction mode, the buckling of the spindle is negligible. The screw jacks cannot safely handle lateral loads. In case of an improperly centered load, a linear bearing should be used to absorb the moment and thus prevent premature wear or failure.

Screw jacks are made of AISI 316 stainless steel, providing good corrosion resistance and resistance against salinity as well as good tensile strength in both low and high operating temperatures [34]. According to Cho et al. [36], the use of a worm screw drive allowed utilizing the irreversibility of the mechanism itself, to keep the lifting mechanism in position without supplying torque and, in this manner, to save energy. During pushing up or down, the load-caused frictional stresses arise in contact between the thread and the slider, which the actuator should overcome. Under certain conditions, vibrations can appear in screw jack mechanisms, during downward motion due to system instability [37].

## THE EFFECT OF LUBRICATION ON THE OPERATION OF SCREW MECHANISM

The screw mechanism can operate under conditions of a lack of lubrication or of lubrication by various greases. Such conditions strongly affect the behavior of the mechanism, its resistance to motion and wear. Various models for the

velocity-dependent COF, which can be useful in the lift jack applications, are available in the literature [38–40]. Such models comprise Coulomb or constant friction, Stribeck friction and viscous or linear friction. Several models are used for the friction compensation [41, 42]. Dry/boundary lubricated conditions in the mentioned contact zone were considered during studies described in [32, 43].

Inside the lead screw friction block, a continuous stick-slip friction model can be applied, allowing for the determination of the friction force and torque coefficients according to the rotation speed of the screw–nut system linked to the joint [44, 45]. An irreversible drive allowed the electric motors to be applied only while maneuvering the operating machine [46]. Smaller values for the velocity threshold and the low-pass filter constant made the model closer to reality but resulted in a numerically stiffer system.

The self-locking condition appeared when the angle of the friction cone exceeded the helix angle. Under static conditions, self-locking can occur when the coefficient of friction reaches a value of 0.017 [33]. The automatic braking condition occurs when the friction energy transmitted from the nut exceeds the energy absorbed by the screw. This takes place at a low feed rate [47] where the COF reaches a value of 0.024. The self-locking action (static condition) does not always result in self-braking action (dynamic condition).

The screw jacks can be lubricated using forced lubrication systems, to single-chamber design, oil-bath lubrication, or programmable units. The exemplary Unimec CU Single Chamber Assembly is a completely sealed, oil-bath configuration for applications where the duty cycle requires constant, continuous lubrication for all moving parts. The programmable lid allows input user's lubrication specifications [34]. Another option, is Unimec Oil Bath Rigid Protection completely sealed and filled with oil, protecting the trapezoidal screw against dust and debris. Each time it descends, the spindle dips into the oil bath for permanent lubrication [34].

The next option is the use of techno-polymers, allowing screw jacks to operate dry in food applications. Such techno-polymers are high-strength plastics with high resistance to heat and mechanical stress. When reinforced with fiberglass, they offer extremely high strength and rigidity as well as good creep resistance. They can operate without lubricants, which is desirable in food industry applications [34].

The exemplary Unimec Aleph Series of trapezoidal screw jacks are made from polyacrylamide – a glass-fiber reinforced techno-polymer. During molding, a pure polymer film forms on the molded component surfaces, providing excellent sliding properties and thus allowing dry operation. Although the techno-polymer is not self-lubricating, the sliding layer of the spindle greatly decreases maintenance downtime and even enhances the lifespan of a screw jack [34]. According to [48], the lubricant should not be corrosive and must have neutral pH. In addition, the lubricant must be oxidation-resistant and non-channeling. Operating temperatures strongly affect the selection of lubricants. UNI-LIFT recommends the following extreme pressure greases or their equivalents:

- For operation up to 82 °C, the Shell Alvania EP2 premium Li based grease should be used. For another brand EP2 grease used, its viscosity should be 840 to 890 SUS at 100 °F, and 76 to 84 SUS at 210 °F.
- For operation up to 204 °C, the Shell Albida EP2 elevated temperature grease should be applied. If another brand of elevated temperature grease is used, it should have a viscosity of 539 SUS at 100 °F.
- For operation down to -73 °C, the Shell Aero-Shell Grease 7 (low temperature aviation synthetic hydrocarbon microgel grease) should be used.
- Standard UNI-LIFT units can operate at 27 °C with a 73 °C temperature rise. For higher temperatures, special seals are required. Special greases approved for food industry applications and greases for very low temperature applications below -73 °C are needed.

The lead screw-nut contact zone can be lubricated with dry PTFE or silicone spray. Constantinou et al. [49] elaborated a mathematical model of the frictional behavior of Teflon sliding bearings accounting for multidirectional motion at the Teflon-steel interface, velocity, and pressure dependence of the coefficient of sliding friction, and breakaway (or static) friction effects. The model was characterized by four parameters, including the minimum and maximum values of the sliding coefficient of friction, the ratio of breakaway to sliding coefficient of friction at the initiation of sliding and a parameter describing the variation of the sliding coefficient of friction with velocity.

Chang et al. [50] proposed an analytical model describing frictional behavior in the contact zone

between Teflon and stainless steel. The model included the influences of normal pressure, its rate and history, sliding distance, sliding velocity and its history, sliding work, etc. The dynamic friction force in the model, independent of both the normal pressure and the sliding velocity, was determined by multiplying the quasi-static friction force by an amplification factor purely affected by the sliding velocity.

According to [51] during frictional tests of steel/steel contact normalized COF trend in function of the sliding velocity for the tests performed at T = 25 °C, normal load equal to 10 N, for the velocity range from 0 to 2 mm/s, lubricated with lithium (LiCPAO) grease was characterized by $\mu_{st}$ = 0.193, $v_0$ = 0.1 mm/s, $\mu_0$ = 0.177, and $\mu_k$ = 0.19 (v = 2 mm/s).

## MATERIALS AND METHODS

The model of the trapezoid scissor car lift was elaborated with a drive via an electric motor (Figure 1a). The model comprises the elastic lift base 1, the elastic lift head 2, four elastic lift arms 3 (two upper and two bottom arranged symmetrically), the rigid lift nut 4 mating with rigid lead screw 5 connected with the rigid shaft c of electric module 6, two elastic pins 7 connecting lift arms, two elastic pins 8 symmetrically connecting lift arm 3 with lift cube 2, two elastic pins 9 symmetrically connecting lift arm 3 with lift base 1. Both rigid and elastic elements were made of stainless steel. For elastic elements, it was assumed the isotropic material model, characterized by a Young's modulus of 210000 MPa, a Poisson Number of 0.3 and a density of 7800 kg/m$^3$. The electric module assembly included a two-piece housing, gear transmission (gears a and b), two shafts c and d, deep groove ball bearings e, internal and external snap rings, a spacer sleeve enabling screwing the motor to the housing, and electric motor 10. Additionally, the housing was equipped with special ears that eliminate the rotational degree of freedom and facilitate mounting of the electrical module.

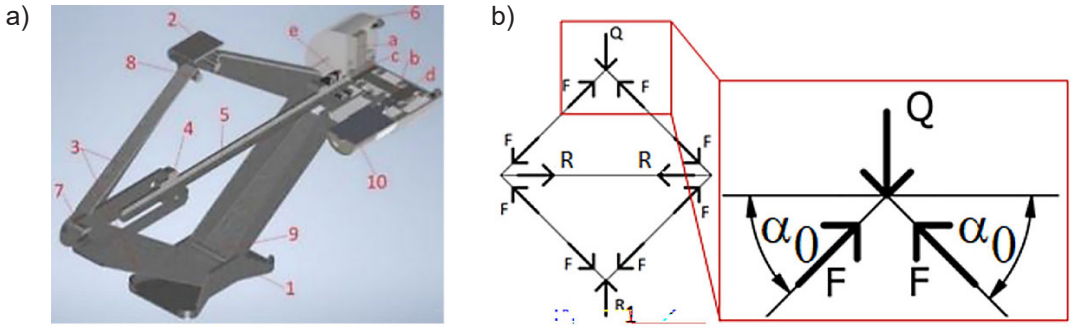


**Figure 1.** a) The scissor car lift with a drive via an electric module; b) the forces in the model of the scissor lift. 1 – lift base, 2 – lift head, 3 – lift arms, 4 – lift nut, 5 – lead screw, 6 – electric module including gear, 7 – pin connecting lift arms, 8 – pin connecting lift arm and lift cube, 9 – pin connecting lift arm and lift base, 10 – electric motor. The course of the motor speed vs. time assumed for the analysis, comprising the motor acceleration in the period from 0–0.06 s, maintaining constant speed in the period from 0.06 to 4.94 s, and breaking to stop in the period from 4.94 to 5 s, is presented in Figure 2.

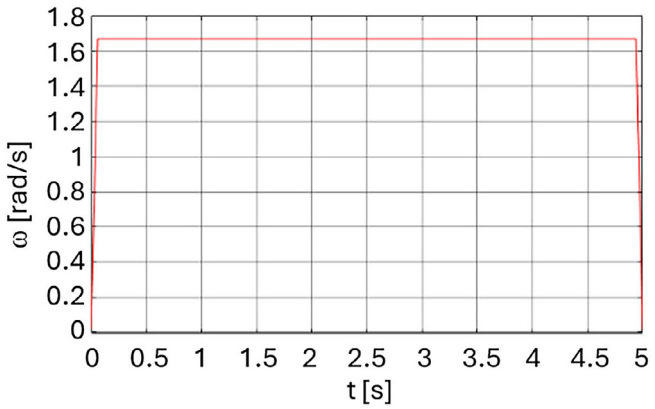


**Figure 2.** The assumed course of the motor speed versus time

An integral part of the model of car lift dynamics is the model of the nut-leading screw assembly. The model of such an assembly (Figure 3) described in [32] was adapted for the current study. The axial force (Figure 1b) varied according to Equation 1:

$$R = \frac{Mg}{\tan\alpha} = \frac{Mg}{\sqrt{\left(\frac{L}{L\cos\alpha_0 - r_m\theta\tan\lambda}\right)^2 - 1}} \quad (1)$$

where: $\alpha_0$ = 15° is an initial (minimum) angle of skew of the scissor arm relative to the axis of the leading screw, corresponding to the minimum lift; $\alpha$ = 90° is a maximum angle of skew of the scissor arm relative to the axis of the leading screw corresponding to the maximal lift.

From Newton's second law applied to the lead screw and nut, Equation 2 for the case of lifting a vehicle was obtained [32]:

$$(I - r_m^2\tan\lambda\,\xi m)\ddot{\theta} + k\theta + (c - r_m^2\tan\lambda\,\xi c_x)\dot{\theta} = \\ = k\theta_i - r_m\xi\left(R - F_0 sgn(\dot{\theta})\right) - T_0 sgn(\dot{\theta}) \quad (2)$$

For the case of lowering a vehicle, such Equation takes the form (3):

$$(I - r_m^2\tan\lambda\,\xi m)\ddot{\theta} + k\theta + (c - r_m^2\tan\lambda\,\xi c_x)\dot{\theta} = \\ = -k\theta_i - r_m\xi\left(R + F_0 sgn(\dot{\theta})\right) + T_0 sgn(\dot{\theta}) \quad (3)$$

where: $m \approx 1$ kg is an average equivalent mass of a translating part, $I = 3 \times 10^{-6}$ kgm$^2$ is a lead screw moment of inertia, $\lambda$ is the lead angle (for the trapezoidal asymmetric thread S12x2, the $\lambda$ = 3.47°), and $r_m$ is the pitch circle radius (for the trapezoidal asymmetric thread S12x2, the $r_m$ = 4.265 mm); $\theta$ is the lead screw rotation; $\theta_i$ is the input rotational displacement applied to the lead screw via a flexible coupling characterized by torsional spring constant $k$; $R$ is the axial force applied to the nut.

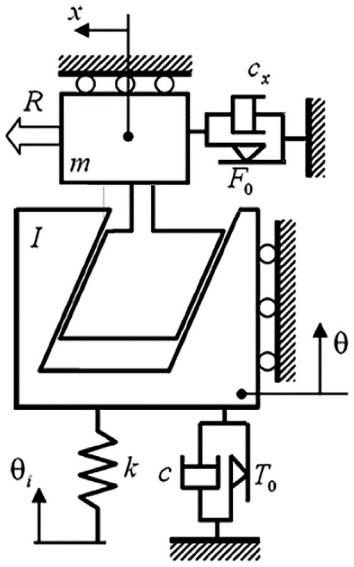


**Figure 3.** The model of nut-leading screw assembly

This force depends on the weight of the lifted solid, on the geometry and varied positions of the lift arms, lift base, and lift head, as well as on their stiffness, the values of which are assumed to be very high. Also, $c = 4 \times 10^{-4}$ Nms/rad is the rotational linear damping coefficient of the lead screw supports, and $c_x = 10^6$ kg/s is the equivalent linear damping coefficient of the whole set of lift arms, lift base and lift head. It was assumed that this coefficient value is close to that characterizing the bearing supporting the translating part in the mechanism studied by [43]. $T_0$ = 0.01 Nm is the frictional torque in the lead screw supports [43]. The equivalent linear damping coefficient of the whole set of lift arms, lift base and lift head can also be determined from Equtaion 4.

$$c_x = 2\zeta\sqrt{k_{eq}m_{eq}} \quad (4)$$

where: $m_{eq}$ – equivalent mass of the loaded lift structure. It was assumed to be close to 1000 kg; $\zeta$ – viscous damping ratio of the construction. For the construction made of steel with joints, such a ratio can reach a value of 0.3 [52], $k_{eq}$ – equivalent stiffness of the modeled loaded lift structure. Such a stiffness was determined from the simplified model of the lift presented in Figure 4.

For simplicity, it was assumed that the model is symmetrical against its geometrical plane parallel to the XZ plane. The steel components of the simplified model of the lift and the boundary conditions are shown in Figure 4a for the angle α equal to 15°, in Figure 5a for the angle α equal to 45°, and in Figure 6a for the angle α equal to 65°, respectively. The lift base bottom surface was fixed. The lift head has been loaded by force $F_{XM}$ = 10000 N corresponding to the lifted solid of mass $M$ equal to 1000 kg. The pins connecting lift arms were loaded by vertical forces of estimated values equal to 10 N corresponding to the action of the weight of the motor-screw-nut assembly and horizontal forces $F_{Xp}$ providing small

displacements $u_{yp}$ of connecting pins along the Y axis. The steady-state analysis was conducted. The grid of finite elements has been shown in Figure 4b for the angle α equal to 15°, in Figure 5b for the angle α equal to 45°, and in Figure 6ba for the angle α equal to 65°, respectively. For the analysis, tetrahedral finite elements with four nodes were utilized, each characterized by three degrees of freedom in the form of displacements along the X, Y and Z axes. Between cylindrical surfaces of connecting pins and mating surfaces of holes in the lift base, lift head and lift arms, the contact elements of frictionless nature were introduced. The stiffness $k_{eq}$ can weaken during lifting the solid of mass $M$; however, such variations were neglected during analysis for simplicity. Therefore, such stiffness was estimated from Equation 5:

$$k_{eq} = \frac{F_{Yp}}{u_{Yp}} \tag{5}$$

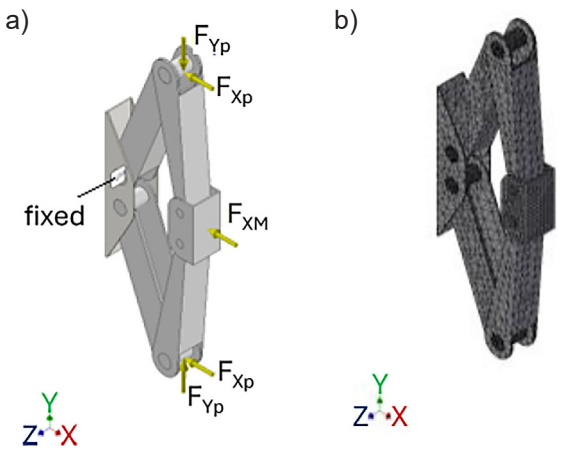


**Figure 4.** The simplified model of the lift: a) components and boundary conditions for the angle α equal to 15°, b) the grid of finite elements

Considering friction resistance in contact zones between connecting pins 7, 8 and 9 and mating hole surfaces in lift arms 3, lift head 2 and lift base 1 (Figure 1), the frictional force acting on the translating part and the lead screw supports can be estimated from Equation 6:

$$F_0 \approx 4\frac{Mg}{2\sin\alpha} = \frac{2\mu_b Mg}{\sin\alpha} \tag{6}$$

where: $\mu_b$ = 0.3 – the COF between pin and lift arm, both made of steel.

To simulate the absence of the effect of friction resistance in such contact zones, COF $\mu_b$ reaches a value equal to 0. The torsional spring was assumed to be equal to 160 Nm/rad, close to the estimated value for the gear motor based on the data given by [53]. COF $\mu_s$ was given by Equation 7 [32]:

$$\mu_s = \mu sgn(\dot{\theta}) \tag{7}$$

The parameter $\xi$ was given by Equation 8 [32]:

$$\xi = \frac{\mu_s - \tan\lambda}{1+\mu_s\tan\lambda} \tag{8}$$

The normal contact force in the lead screw-nut contact zone was obtained from Equation 9 [32]:

$$N = \frac{\left(R - F_0 sgn(\dot{\theta})\right)I + mr_m\tan\lambda\left[k(\theta-\theta_i)+\left(c-r_m^2\tan\lambda\xi c_x\right)\dot{\theta}+T_0 sgn(\dot{\theta})\right]}{(\cos\lambda+\mu_s\sin\lambda)\left(I-r_m^2\tan\lambda\xi m\right)} \tag{9}$$

The torque of resistance to motion $T_r$ of the nut against the lead screw was obtained from Equation 10 [32].

$$T_r = \mu_s N r_m \tag{10}$$

In the present study, the Tustin model (11) for COF was adapted [32]:

$$\mu = \widetilde{\mu_1} + \widetilde{\mu_2}\left(e^{-(|v_s|/v_0)} - 1\right) + \widetilde{\mu_3}|v_s| \tag{11}$$

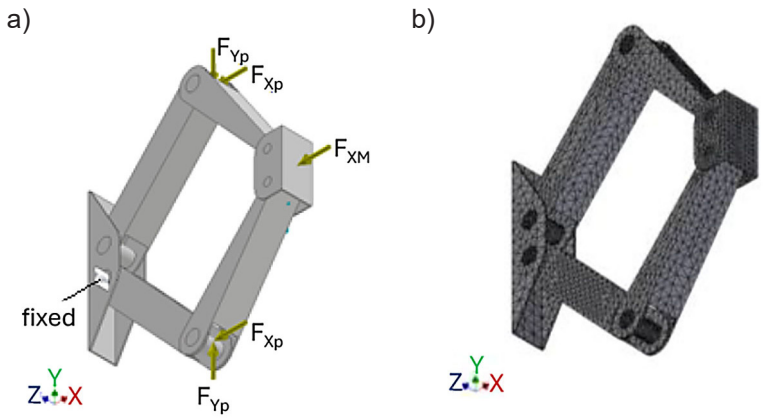


**Figure 5.** The simplified model of the lift: a) components and boundary conditions for the angle α equal to 45°, b) the grid of finite elements

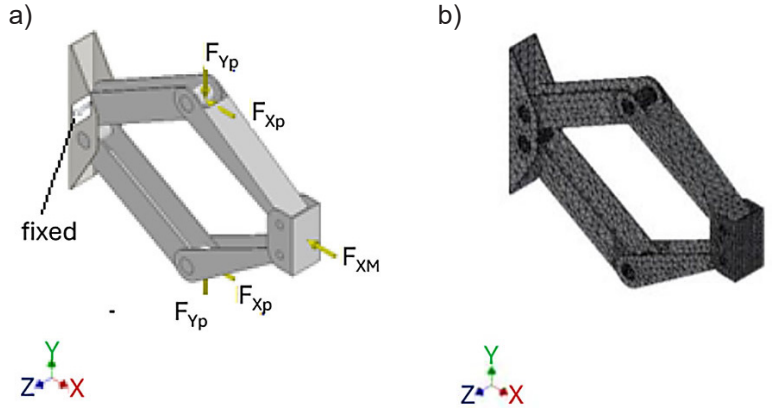


**Figure 6.** The simplified model of the lift: a) components and boundary conditions for the angle α equal to 65°, b) the grid of finite elements

where: $\widetilde{\mu_1}, \widetilde{\mu_2}, \widetilde{\mu_3}$ represented Coulomb, Stribeck, and viscous friction coefficients, respectively; $v_s$ is the relative sliding velocity between contacting nut threads and lead screw threads. Also, $v_0$ controlled the velocity range of the Stribeck effect.

The schematic plot of the velocity-dependent COF was shown in Figure 7. The sliding velocity can be expressed as given by Equation 12:

$$v_s = \frac{r_m}{\cos\lambda}\dot{\theta} \tag{12}$$

During experiments on nut-screw assembly described in [43] the following parameters of the modified friction model (13) were introduced:

$$\mu = \mu_1 + \mu_2\left(e^{-r_0|\dot{\theta}|}\right) + \mu_3|\dot{\theta}| \tag{13}$$

where: $\mu_1 = \widetilde{\mu_1} - \widetilde{\mu_2}, \mu_2 = \widetilde{\mu_2}, \mu_3 = \widetilde{\mu_3}(r_m/\cos\lambda)$, $r_0 = r_m/(v_0\cos\lambda)$.

In this study, the parameters characterized boundary frictional conditions in contact between a lead screw and a nut were close to those used during studies described in [43], namely: $\mu_1$ = 0.218, $\mu_2$ = 0.02, $\mu_3$ = -4.47 × $10^{-4}$ s/rad, and $r_0$ = 0.38 s/rad. To evaluate the effect of lubrication on the frictional conditions in the contact zone between a lead screw and a nut, two lubricants were considered. The contact lubricated with PTFE dry spray was simulated using the parameters of Constantinou et al. model (14) [49] for contact pressure $p$ = 9.36 MPa, temperature of 20 °C, and velocity determined by Equation 12, namely $\mu_{min}$ = 0.0843, $\mu_{max}$ = 0.1961, $\vartheta$ = 0.02.

$$\mu = \mu_{max} - (\mu_{max} - \mu_{min}) \cdot e^{-\vartheta v_s} \tag{14}$$

The contact lubricated with lithium grease with an amount providing mixed friction conditions was simulated using the friction model described by Equation 12 and model parameters $\widetilde{\mu_1}$ = 0.193, $\widetilde{\mu_2}$ = 0.177, $\widetilde{\mu_3} = \frac{0.19-0.177}{2-0.1} \cdot 10^3$ [$\frac{s}{m}$], $v_0$ = 0.1 mm/s [51]. The set of Equation 1–14 has been solved with the software MATLAB Simulink using the Fixed-Step Continuous Explicit Solver based on the Bogacki-Shampine formula [54].

## RESULTS

The distribution of calculated values of displacement along the Y axis for elements of simplified models of lift (Figures 4, 5 and 6) was presented in Figure 8a for the angle α equal to 15°, in Figure 9a for the angle α equal to 45°, and in Figure 10a for the angle α equal to 65°, respectively. Corresponding displacements $u_{Yp}$ of connecting pins along the Y axis were shown in Figures 8b, 9b and 10b, respectively.

Figure 11 shows the force S loading the lead screw as a function of the angle α (Figure 1b). Table 1 presents values of displacement $u_{Yp}$ stiffness $k_{eq}$ calculated from Equation 12, and the damping coefficient $c_x$ calculated from Equation 11 for the angle α and corresponding value of the force $F_{Yp}$ (read from Figure 11, as $F_{Yp}$ corresponds directly to the force $S$).

The estimated course of the damping coefficient $c_x$ vs. angle α was presented in Figure 12. From Table 1 and Figure 12, it is evident that with increasing values of the angle α, the damping coefficient $c_x$ values decrease nonlinearly with a tendency to stabilize.

The obtained course of the friction torque $T$ in contact between a lead screw and a nut under dry/boundary friction conditions as a function of

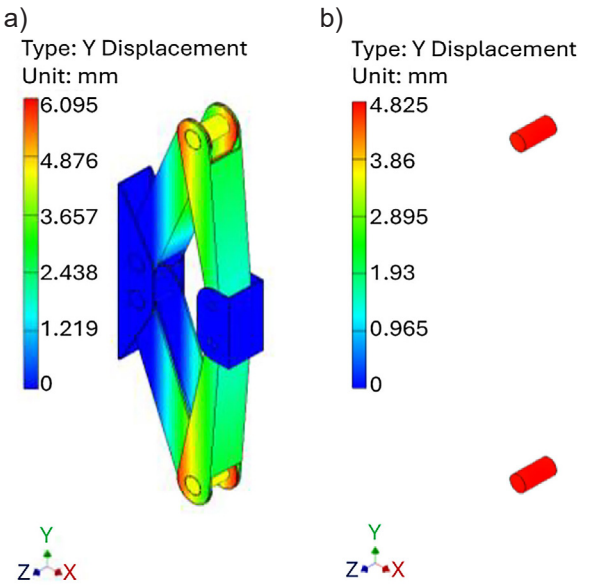


**Figure 8.** The distribution of calculated values of displacement $u_{Yp}$ along the Y axis for the angle α equal to 15° for: a) all components of the simplified model of lift (Figure 4), b) connecting pins

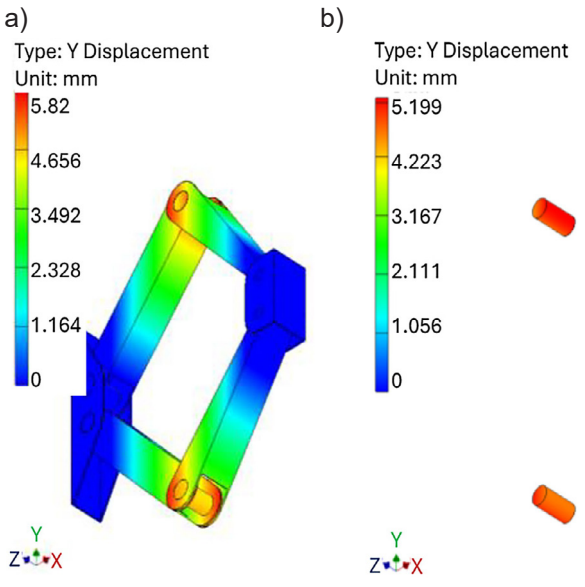


**Figure 9.** The distribution of calculated values of displacement $u_{Yp}$ along the Y axis for the angle α equal to 45° for: a) all components of the simplified model of lift (Figure 5), b) connecting pins

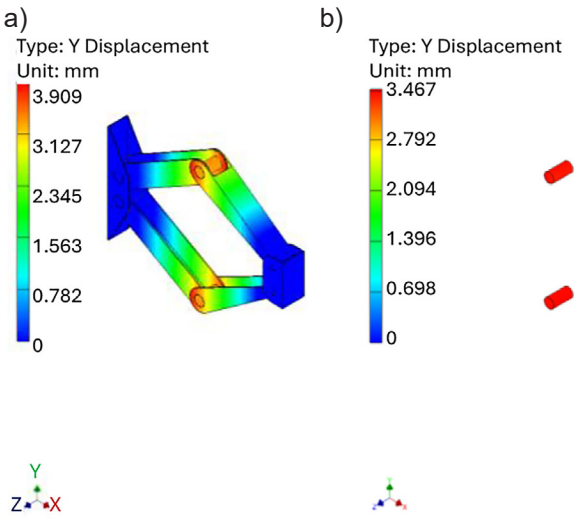


**Figure 10.** The distribution of calculated values of displacement $u_{Yp}$ along the Y axis for the angle α equal to 65° for: a) elements of the *f* simplified model of lift (Figure 6), b) connecting pins

time for the assumed course of the motor speed vs. time during lifting vehicle started from the initial value of angle α equal to 15° was presented in Figure 13a. The enlarged part of the latter was shown in Figure 13b for the period 0.999–1 s. With an increase in time, the friction torque lowered due to reduced contact pressure caused by lowered value of the force loading the contact zone due to changing values of angle α (Figure 1b). In the mentioned period, the motor speed $\omega$ is fixed (Figure 2). When initially the speed $\omega$ raises with increasing time (Figure 2), the numerical effect of the calculation algorithm used by the program may become apparent. This influenced the elevated level of the angle difference $\theta$–$\theta_i$, in relation to which the oscillations of the value of this difference occur. Such oscillations resulted, inter alia, from the stick-slip

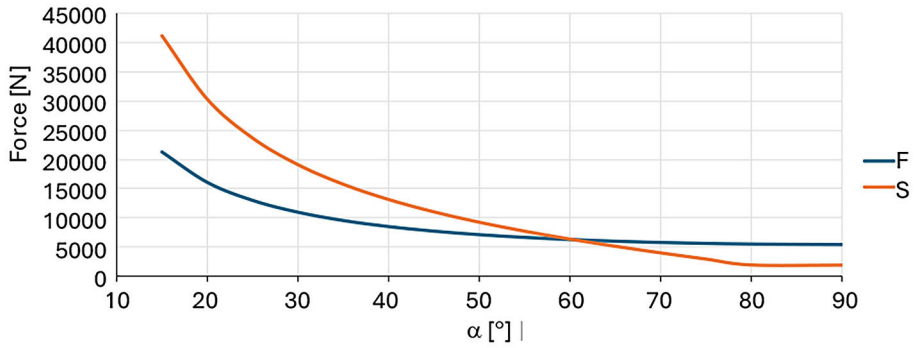


**Figure 11.** Forces F and S loading the lift arm and the lead screw, respectively, vs. the angle α

**Table 1.** The obtained values of the displacement $u_{Yp}$, the stiffness $k_{eq}$, and the damping coefficient $c_x$ for the angle α, and corresponding value of the force $F_{Yp}$

| α [°] | $F_{Yp}$ [N] | $u_{Yp}$ [mm] | $k_{eq}$ [N/mm] | $c_x$ [kg/s] |
|---|---|---|---|---|
| 15 | 45700 | 4.8 | 9520 | 58544 |
| 45 | 11580 | 5.1 | 2316 | 28878 |
| 65 | 5820 | 3.9 | 1492 | 23175 |

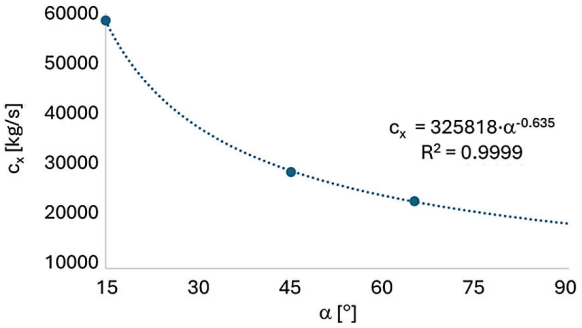


**Figure 12.** The estimated course of the damping coefficient $c_x$ vs. the angle α

phenomena occurring during simulations. These phenomena are visible in Figure 13c, which contains the course of the angle difference $\theta–\theta_i$ as a function of time $t$, for the same period as in the case of Figure 13b. Such phenomena also occurred during studies on the screw-nut assembly reported in [43]. The course of the friction torque $T$ versus time for the COF $\mu_b$ value equal to 0 was shown in Figure 13d. Obtained values of friction torque $T$ were at least threefold lower than in the case of $\mu_b$ value equal to 0.3, which confirmed a significant role of the friction resistance in contact zones linked to the connecting pins of the lift. The enlarged part of Figure 13d was shown in Figure 13e for the period 0.999–1 s. The stick-slip phenomena, although with a smaller amplitude, occurred during simulations, as shown in Figure 13f, which contains the course of the angle difference $\theta–\theta_i$ as a function of time $t$. During lifting, the vehicle started from the initial value of angle α equal to 45° the course of the friction torque versus time was shown in Figure 13g, while during lowering in 13j. The enlarged parts of these figures were shown in Figures 13h and 13k, respectively, for the period 0.999–1 s. For this value of angle α, the calculated values of the friction torque $T$ were up to five-fold lower compared to the lifting case started from the initial angle α value equal to 15°. It was due to much lower values of the force $S$ loading the contact zone between lead screw and a nut. During lowering the vehicle, the friction torque $T$ values slightly increased with time. The stick-slip phenomena, with exceedingly small amplitude were visible in Figures 13i and 13l containing the courses of the angle difference $\theta–\theta_i$ as a function of time $t$. During lifting, the vehicle started from the initial value of angle α equal to 65°. The course of the friction torque $T$ versus time was shown in Figure 13m, while during lowering in Figure 13p. The enlarged parts of those figures were shown in Figures 13n and 13q, respectively, for the period 0.999–1 s. For this value of angle α the calculated values of the friction torque $T$ were up to ten-fold lower compared to the lifting case started from the initial angle α value equal to 15°. It also resulted from the much lower values of the force $S$ loading the contact zone between the lead screw and a nut. During lowering of the vehicle, the friction torque $T$ values also slightly increased with time. The stick-slip phenomena, with an exceedingly small amplitude are visible in Figure 13o and non-visible in Figure 13r containing the courses of the angle difference $\theta–\theta_i$ as a function of time .

The obtained course of the friction torque $T$ in the same contact zone under lubrication by PTFE dry spray as a function of time for the assumed course of the motor speed $\omega$ vs. time $t$ was shown in Figure 14. For lubrication using lithium grease, such a course was shown in Figure 15. The similar tendencies in changing the friction torque $T$ values with time were observed for the corresponding consecutive cases shown in Figures 13a-r. In both cases with an increase of time, the friction torque $T$ values also decreased due to lowered contact pressure caused by the reduced value of the force loading the contact zone due to changing values of angle α (Figure 1b). In the case of PTFE-based lubricant the values of the friction torque can be over twice lower compared to the case of dry/boundary friction conditions in the analyzed contact

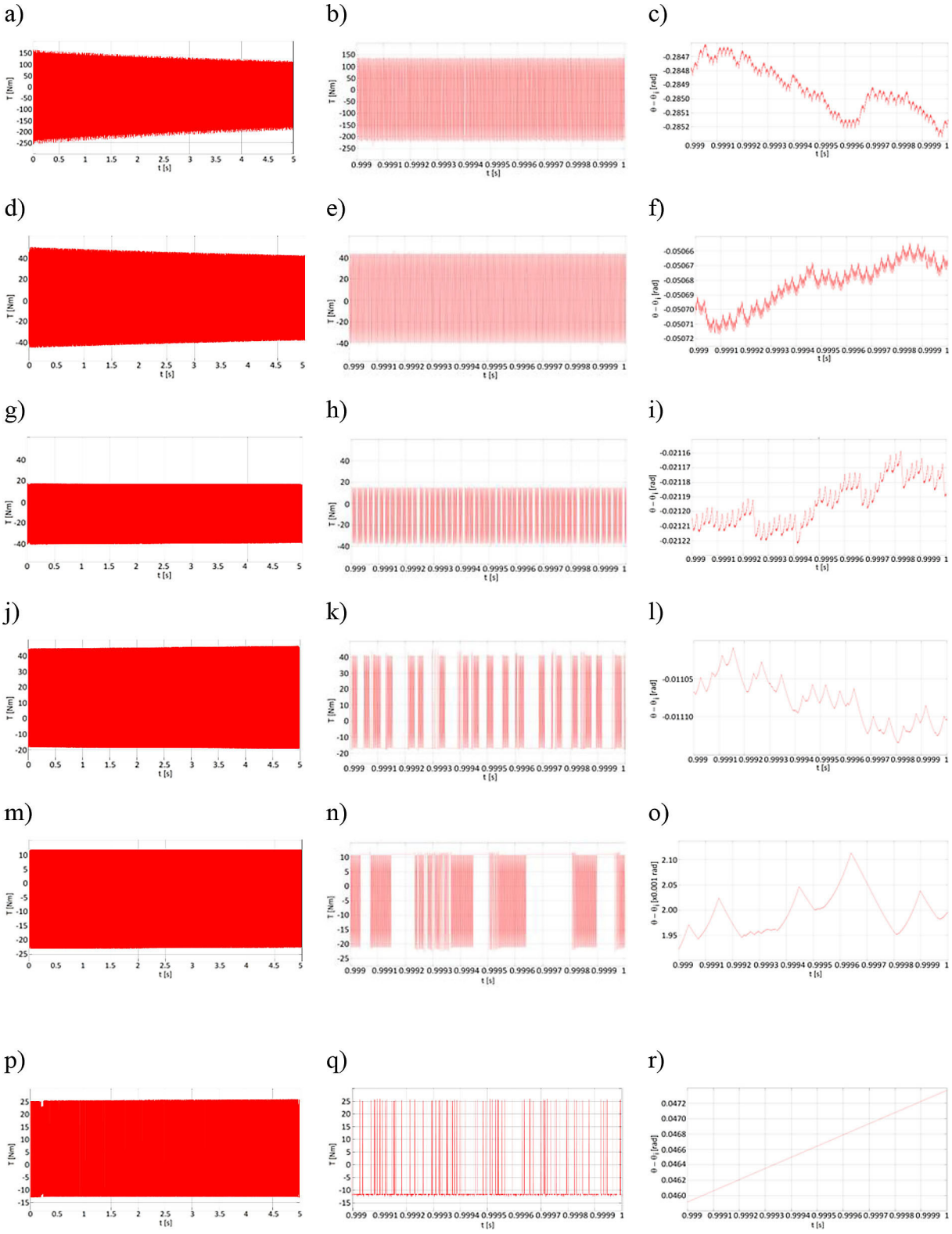


**Figure 13.** The course of the friction torque $T$ in the lead screw-nut contact zone vs. time $t$ for the assumed course of the motor speed $\omega$ vs. time $t$ for dry/boundary friction conditions during: a) lifting started from the angle α of 15° and COF $\mu_b$ of 0.3, d) lifting started from the angle α of 15° and COF $\mu_b$ of 0, g) lifting started from the angle α of 45° and COF $\mu_b$ of 0.3, j) lowering started from the angle α of 45° and COF of 0.3, m) lifting started from the angle α of 65° and COF $\mu_b$ of 0.3, p) lowering started from the angle α of 65° and COF $\mu_b$ of 0.3. The enlarged fragments of the figures for the period 0.999-1s: b) relative to Figure 13a, e) relative to Figure 13d, h) relative to Figure 13f, k) relative to Figure 13j, n) relative to Figure 13m, q) relative to Figure 13p. The courses of the angle difference as a function of time : c) relative to Figure 13b, f) relative to Figure 13e, i) relative to Figure 13h, l) relative to Figure 13k, o) relative to Figure 13n, r) relative to Figure 13q.

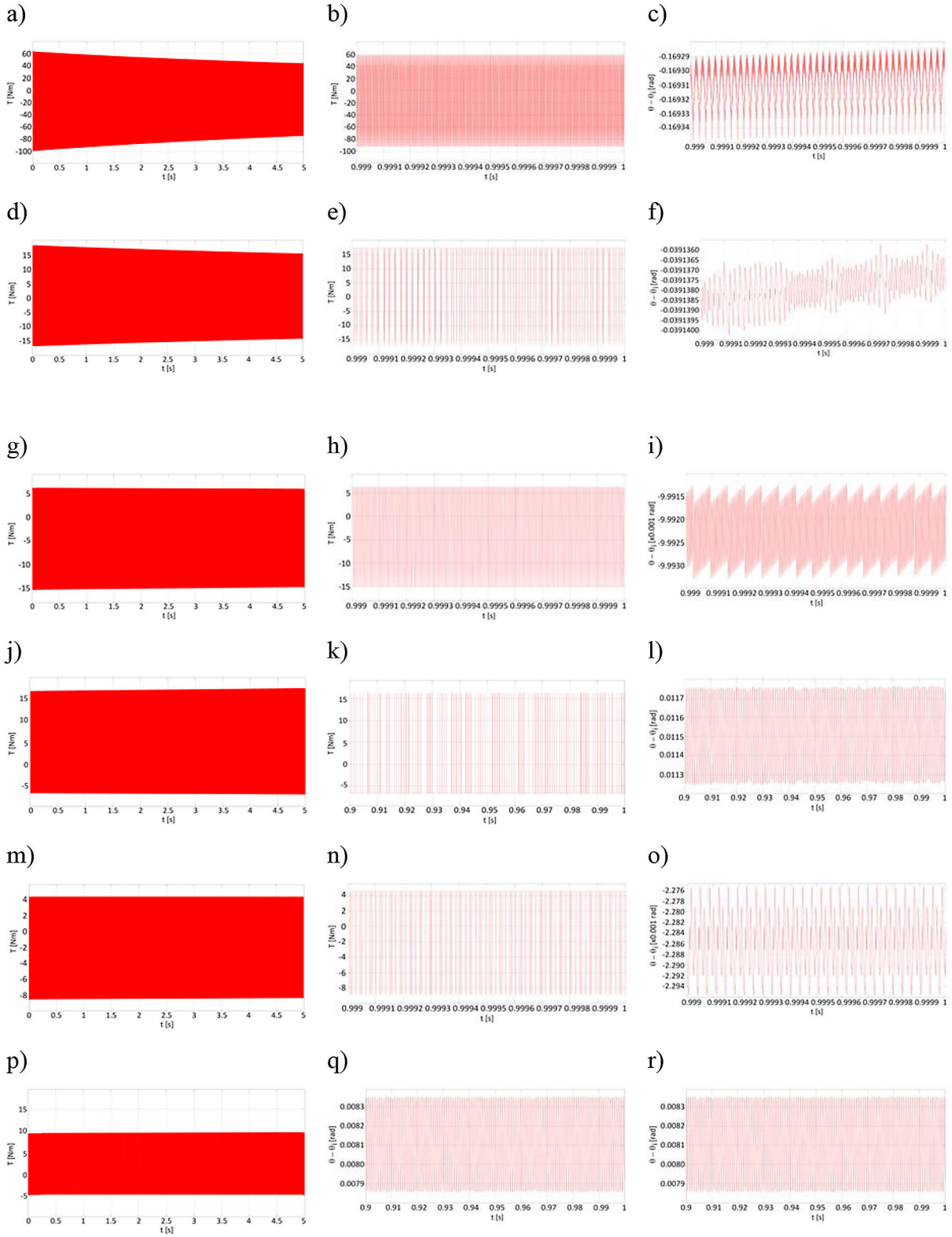


**Figure 14.** The course of the friction torque $T$ in the lead screw-nut contact zone vs. time $t$ for the assumed course of the motor speed $\omega$ vs. time $t$ for lubrication by PTFE dry spray during: a) lifting started from the angle α of 15° and COF $\mu_b$ of 0.3, d) lifting started from the angle α of 15° and COF $\mu_b$ of 0, g) lifting started from the angle α of 45° and COF $\mu_b$ of 0.3, j) lowering started from the angle α of 45° and COF  of 0.3, m) lifting started from the angle α of 65° and COF $\mu_b$ of 0.3, p) lowering started from the angle α of 65° and COF $\mu_b$ of 0.3. The enlarged fragments of the figures for the period 0.999–1 s: b) relative to Figure 14a, e) relative to Figure 14d, h) relative to Figure 14f, k) relative to Figure 14j (for period 0.9–1 s), n) relative to Figure 14m, q) relative to Figure 14p (for period 0.9–1 s). The courses of the angle difference  as a function of time : c) relative to Figure 14b, f) relative to Figure 14e, i) relative to Figure 14h, l) relative to Figure 14k, o) relative to Figure 14n, r) relative to Figure 14q

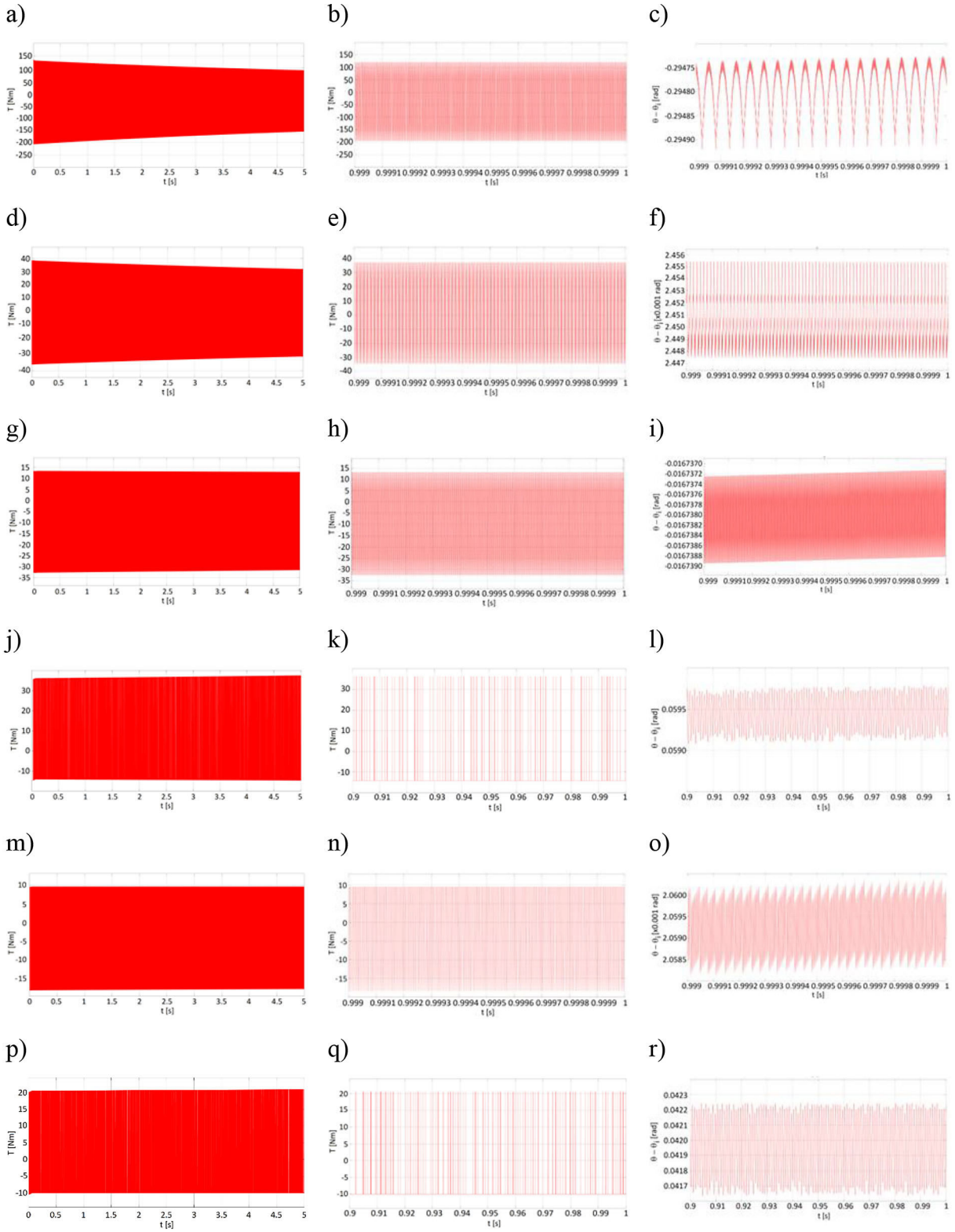


**Figure 15.** The course of the friction torque $T$ in the lead screw-nut contact zone vs. time $t$ for the assumed course of the motor speed $\omega$ vs. time $t$ for lubrication by lithium grease during: a) lifting started from the angle α of 15° and COF of 0.3, d) lifting started from the angle α of 15° and COF $\mu_b$ of 0, g) lifting started from the angle α of 45° and COF $\mu_b$ of 0.3, j) lowering started from the angle α of 45° and the COF $\mu_b$ of 0.3, m) lifting started from the angle α of 65° and COF $\mu_b$ of 0.3, p) lowering started from the angle α of 65° and COF $\mu_b$ of 0.3. The enlarged fragments of the figures for the period 0.999–1 s: b) relative to Figure 15a, e) relative to Figure 15d, h) relative to Figure 15f, k) relative to Figure 15j (for period 0.9–1 s), n) relative to Figure 15m, q) relative to Figure 15p (for period 0.9–1 s). The courses of the angle difference as a function of time : c) relative to Figure 15b, f) relative to Figure 15e, i) relative to Figure 15h, l) relative to Figure 15k, o) relative to Figure 15n, r) relative to Figure 15q

zone. In the case of lithium grease, the obtained changes in values of the friction torque were by 20% lower compared to the case of dry/boundary friction conditions in the analyzed contact zone. The stick-slip phenomena occurred during simulations (Figures 14c, 14f, 14l, 14o, 14r and 15c, 15f, 15l, 15o, 15r), however, most often with smaller magnitudes than in the case of dry friction.

## CONCLUSIONS

The friction behavior in contact zone between the lead screw and mating nut exhibited complex nature. In both cases of lack of lubricant and lubricated contact zones, the stick-slip phenomenon occurred therein. Under lubrication the magnitudes of such oscillations were most often smaller compared to the case of dry friction in contact zones. For all analyzed cases during lifting the vehicle, the friction torque $T$ values decreased due to lowered contact pressure caused by the reduced value of the force loading the contact zone due to changing values of angle $\alpha$. Conversely, during lowering the vehicle, the friction torque $T$ values slightly increased due to reduced values of the force loading the contact zone of the lead screw-nut with changing values of angle $\alpha$. In the case of PTFE-based lubricant the values of the friction torque $T$ were less than half of the values for dry or boundary friction conditions in the analyzed contact zone. The use of lithium grease can provide a 20% reduction in the friction torque values compared to the case of dry/boundary friction conditions in such a contact zone. For lower-speed operations, the sliding system like a lead screw-nut can be preferentially lubricated by periodically applying grease to the shaft by hand or using the lubrication hole on the Lead Screw Nut. THK recommends the application of lithium grease The computational models used for the resistance to motion in the screw-nut contact were verified for accuracy by borrowing them from published experimental studies conducted for other contact conditions between the mating surfaces. Because the current study involves a prototype device not equipped with the necessary measurement equipment, the obtained resistance to motion values in the screw-nut contact have not yet been verified and will be the subject of further research.

## REFERENCES


1. Skrzymowski W. Podnośniki pojazdów/Vehicle lifts. 2nd Ed. Krosno, Poland: KaBe; 2017. https://www.naukowa.pl/Ksiazki/podnosniki-pojazdow-1629728
2. Liftnow. What Are the Different Types of Vehicle Lifts? 2024. https://liftnow.com/types-of-vehicle-lifts/
3. Michałowski P. What type of car lift fits the workshop most? SiegStar. 2024. https://siegstar.com/en/article/what-type-of-car-lift-fits-the-workshop-most/
4. Kroemer Car Lift. Scissor lifts for your workshop from Krömer. 2024. https://kroemer-car-lift.co.uk/car-scissor-lift.html
5. Muneer A. Hydraulic Car Lifts: Understanding Their Types, Uses, and Benefits. Medium. 2023. https://medium.com/@muneer-ahammed/hydraulic-car-lifts-understanding-their-types-uses-and-benefits-4e7b3c333c98
6. JMC Automotive Equipment. Vehicle Lifts: Different Types and how to Choose the Right One. 2024. https://jmcautomotiveequipment.com/pages/jmc-equipment-buyers-guide/vehicle-lifts-different-types-and-how-to-choose-the-right-one.html
7. Hongyu T, Ziyi Z. Design and Simulation Based on Pro/E for a Hydraulic Lift Platform in Scissors Type. Procedia Engineering. 2011;16:772–81.
8. Azinee SN, Zakaria MK, Atika NS, Norsilawati N, Aminullah ARM, Ibrahim Mh. Design Analysis and Topology Optimization for Scissor Car Jack Using Static Linear Approch. I tech mag. 2019 Oct 1 [cited 2025 Jul 23];19–22. http://itechmag.org/paper/volume%201/19-22.pdf
9. Oghoghorie O, Osaretin JO. Design and fabrication of an automated scissors car jack to lift and lower a car with minimal human effort. Journal of Applied Sciences and Environmental Management Supplementary. 2024;28(11B).
10. Abuzied H, Abo ELnaga Y. Bluetooth Operated Scissor Jack: The Future of Vehicle Lifting Equipment for Developing Countries. JMET Journal UTeM. 2024 Jun 17;16(1):15–24. https://jmet.utem.edu.my/jmet/article/view/6377
11. Nadzri Wanwa, Harudin N. Design and development of automatic scissor type car jack. 2023 Jun;1(1):16–25. https://semarakilmu.my/index.php/sej/article/view/286/451
12. Babu S, Reddy BhBC, Vamsi MB, Bharagv T, Chaitanya AK, Ramana KV. Fabrication of an innovative scissor jack. Indian Streams Research Journal. 2015;5(4):1–8.
13. Ajayi AB, Adeyinka MO. Development of an Automatic Scissors Screw Car Jack. AJERD. 2024 Aug 24;7(2):193–206. https://journals.abuad.edu.ng/

index.php/ajerd/article/view/486

14. Pratheep VG, Tamilarasi T, Ravichandran K, Srinivasan M, Someswaran N, Vimal S, Praveen S. Design and fabrication of IOT based scissor jack. In Timisoara, Romania; 2023, 020002. http://aip.scitation.org/doi/abs/10.1063/5.0148663
15. Bzura P. Analysis and evaluation of oil lubricity from the viewpoint of energy apects and of the tribological system action. Scientific Journals of the Maritime University of Szczecin, Zeszyty Naukowe Akademii Morskiej w Szczecinie. 2009;17(89):20–4.
16. Faulve MNM. Design and Development of a Screw Jack: An Input Repair Tool for Light Vehicles. AIR. 2024 Jan 18;25(1):105–16. https://journalair.com/index.php/air/article/view/1023
17. Atif M, Mumtaz F, Adeel M. Design and fabrication of a motorized screw jack. IET Conf Proc 2023 Feb 23; 2022(26):114–9. http://digital-library.theiet.org/doi/10.1049/icp.2023.0358
18. Nedžad Repčić, Isad Šarić, Avdić V. Theoretical Reviews on how to Improve the Degree of Efficiency on Power Screws. 2012; http://rgdoi.net/10.13140/RG.2.1.2728.4248
19. Abdulafeez O, V. SOC, O. MK, C. DP. Development and Performance Investigation of a Laboratory Screw Jack. ijird. 2021 Jan 31;10(1). http://www.internationaljournalcorner.com/index.php/ijird_ojs/article/view/157839
20. Ezurike B, Okwu M. Modified Screw Jack for Lifting Operation in Industrial Setting. IJET. 2017 Dec 29;13:39–50. https://www.academicoa.com/IJET.13.39
21. Akinwonmi AS, Mohammed A. Modification of the existing design of a car jack. Journal of Emerging Trends in Engineering and Applied Sciences. 2012;3(4):581–8.
22. Shejwal OV, Bhave MD, Karande RD. Analysis and modification of screw jack body using finite element analysis. International Journal of Science Technology & Engineering. 2017;3(7):103–6.
23. Muhammed Y, Bekele Y, Abebaw M. Design of Screw Car Jack. Design. Mechanical Engineering Department, Institute of Technology, University of Gondar, Ethiopia; 2022.
24. Khatwate VinayakH, Kunder L, Talekar S, Lay D, Angadikar S. Optimization of power screw material used in screw jack. International Journal of Emerging Trends in Research. 2022;SI I:78–89.
25. De Simone MC, Veneziano S, Guida D. Design of a Non-Back-Drivable Screw Jack Mechanism for the Hitch Lifting Arms of Electric-Powered Tractors. Actuators. 2022 Dec 2;11(12):358. https://www.mdpi.com/2076-0825/11/12/358
26. Patil MR, Kachave SD. Design and analysis of scissor jack. Int J Mech Eng & Rob Res. 2015;4(1):327–35.
27. Pervan N, Muminović A, Muminović A, Delić M. Development of parametric CAD model and structural analysis of the car jack. Adv Sci Technol Res J. 2019 Sep 1;13(3):24–30. http://www.journalssystem.com/astrj/Development-of-parametric-CAD-model-and-structural-analysis-of-the-car-jack,109791,0,2.html
28. Ayai T, Jacob GD, Shameer A, Ramalingam D. Design and fabrication of devising simplified motorized scissor jack. International Journal of Management, Technology and Engineering. 2018;8(8):2007–14.
29. Tambari S, Lemii P, Sorbari K, Lelesi N. Experimental investigation of the performance of a laboratory screw jack. IOSR Journal of Mechanical and Civil Engineering, 2015 Aug;12(4 v.II):16–26.
30. Coates M. Lead Screw Coatings. Thomson Linear. 2024. Available from: https://www.thomsonlinear.com/downloads/articles/Lead_Screw_Coatings_taen.pdf
31. Sharifov ZZ, Bashirov FR. Change of composition and structure of diffusion chrome coating during friction. Scientific Journals of the Maritime University of Szczecin, Zeszyty Naukowe Akademii Morskiej w Szczecinie. 2013;33(105):96.
32. Vahid-Araghi O, Golnaraghi F. Chapter 5 - Mathematical Modeling of Lead Screw Drives. In: Friction-Induced Vibration in Lead Screw Drives. New York, NY: Springer New York; 2011. http://link.springer.com/10.1007/978-1-4419-1752-2
33. De Simone MC, Veneziano S, Guida D. Design of a non-back-drivable screw jack mechanism for the hitch lifting arms of electric-powered tractors. Actuators. 2022 Dec 2;11(12):358.
34. Bronzini A. A Guide to trapezoidal screw jack design, construction and selection. Power Transmission Engineering Magazine. 2023 Jun 5; https://www.powertransmission.com/articles/9282-a-guide-to-trapezoidal-screw-jack-design-construction-and-selection
35. Kelkston Actuation Ltd. Screw Jack Selection. 2023. https://www.kelstonactuation.com/upl/standard/kelston_screw-jack-selection.pdf
36. Cho MS, Hwang HS, Lee MH, Kim B, Zinn MR. A screwjack mechanism based separation device driven by a piezo actuator. Int J Precis Eng Manuf. 2012 Nov;13(11):2079–82.
37. Gallina P. Vibration in screw jack mechanisms: experimental results. Journal of Sound and Vibration. 2005 Apr;282(3–5):1025–41.
38. Niranjan P, Karinka S, Sairam KVSSSS, Upadhya A, Shetty S. Friction modeling in servo machines: a review. Int J Dynam Control. 2018 Sep;6(3):893–906.
39. Rybkiewicz M, Leus M. Selection of the friction model for numerical analyses of the impact of longitudinal vibration on stick-slip movement. Adv Sci Technol Res J. 2021 Sep 1;15(3):277–87.

40. Shen MM, Yang XD. Modeling of joint structure interface friction mechanics: A review. Advances in Mechanics. 2024;
41. Ruan W, Dong Q, Zhang X, Li Z. Friction compensation control of electromechanical actuator based on neural network adaptive sliding mode. Sensors. 2021 Feb 22;21(4):1508.
42. Ko D, Lee D, Chung WK, Kim K. Bounded Compensation with Friction Estimation for Accurate Motion Tracking and Compliant Behavior of Industrial Manipulators. In: 2023 IEEE International Conference on Robotics and Automation (ICRA). London, United Kingdom: IEEE; 2023]. 5235–41. https://ieeexplore.ieee.org/document/10160818/
43. Vahid-Araghi O, Golnaraghi F. Chapter 9 An Experimental Case Study. In: Friction-Induced Vibration in Lead Screw Drives. New York, NY: Springer New York; 2011. http://link.springer.com/10.1007/978-1-4419-1752-2
44. De Simone M, Guida D. Modal coupling in presence of dry friction. Machines. 2018 Feb 27;6(1):8.
45. Formato A, Ianniello D, Pellegrino A, Villecco F. Vibration-Based Experimental Identification of the Elastic Moduli Using Plate Specimens of the Olive Tree. Machines. 2019 Jun 20;7(2):46.
46. Noormohamed A, Mercan O, Ashasi-Sorkhabi A. Optimal active control of structures using a screw jack device and open-loop linear quadratic gaussian controller. Front Built Environ. 2019 Apr 12;5:43.
47. Niemann, G, Winter H, Höhn BR. Manuale degli organi delle macchine Tecnologie industriali. Tecniche Nuove; 2006. 1056 p.
48. UNI-LIFT. Mechanical Screw Jacks. M and B Series Models. 2020 Jan. Report No.: L2943. https://joycedayton.com/sites/default/files/pdfs/L2943_Instruction_Sheet_M_and_B_Series_01222020a.pdf
49. Constantinou M, Mokha A, Reinhorn A. Teflon Bearings in Base Isolation II: Modeling. J Struct Eng. 1990 Feb;116(2):455–74.
50. Chang KC, Hwang JS, Lee GC. Analytical model for sliding behavior of Teflon-stainless steel interfaces. J Eng Mech. 1990 Dec;116(12):2749–63.
51. Ghezzi I, Tonazzi D, Rovere M, Le Coeur C, Berthier Y, Massi F. Frictional behaviour of a greased contact under low sliding velocity condition. Tribology International. 2021;155:106788.
52. Orban F. Damping of materials and members in structures. J Phys: Conf Ser. 2011 Jan 1;268:012022. https://iopscience.iop.org/article/10.1088/1742-6596/268/1/012022
53. Miller D, Knight B, Miller D, Knight B. Direct drive vs. geared rotary servomotor: A quantification of design advantage: Part 2. Plant Engineering. 2021 Jan 19;1/2021. https://www.plantengineering.com/articles/direct-drive-vs-geared-rotary-servomotor-a-quantification-of-design-advantage-part-2/
54. Matlab Help Center. Fixed Step Solvers in Simulink. Mathworks; 2025. https://www.mathworks.com/help/simulink/ug/fixed-step-solvers-in-simulink.html
55. THK. Lead Screw Nut. Point of Design.. THK; 2024. https://tech.thk.com/en/products/pdf/en_a16_014.pdf